Nuclear Science and Techniques (2025) 36:53
https://doi.org/10.1007/s41365-024-01608-w

Acceptance effect on the $N_t N_p/{N_d}^2$ ratio of light nuclei coalescence yields as a probe of nucleon density fluctuations

An Gu[1,2] · Michael X. Zhang[3]

Received: 23 January 2024 / Revised: 9 August 2024 / Accepted: 13 September 2024 / Published online: 13 February 2025

Abstract

A coalescence model was employed to form deuterons (d), tritons (t), and helium-3 (^{3}He) nuclei from a uniformly-distributed volume of protons (p) and neutrons (n). We studied the ratio $N_t N_p/N_d^2$ of light nuclei yields as a function of the neutron density fluctuations. We investigated the effect of finite transverse momentum (p_T) acceptance on the ratio, in particular, the "extrapolation factor" (*f*) for the ratio as a function of the p_T spectral shape and the magnitude of neutron density fluctuations. The nature of *f* was found to be monotonic in p_T spectra "temperature" parameter and neutron density fluctuation magnitude; variations in the latter are relatively small. We also examined *f* in realistic simulations using the kinematic distributions of protons measured from the heavy-ion collision data. The nature of *f* was found to be smooth and monotonic as a function of the beam energy. Therefore, we conclude that extrapolation from limited p_T ranges does not create, enhance, or reduce the local peak of the $N_t N_p/N_d^2$ ratio in the beam energy. Our study provides a necessary benchmark for light nuclei ratios as a probe for nucleon density fluctuations, an important observation in the search for the critical point of nuclear matter.

Keywords Heavy-ion collision · Critical point · Light nuclei coalescence · Nucleon density fluctuations

1 Introduction

Matter comprises quarks and gluons, which are the most fundamental constituents of nature, together with leptons and gauge bosons. The interactions between quarks and gluons are governed by quantum chromodynamics (QCD). At low temperatures or matter densities, quarks and gluons are confined in hadrons, whereas at high temperatures or matter densities, they are deconfined in an extended volume called the quark–gluon plasma (QGP). The phase transition at low temperature and high matter density is first-order, and at high temperature and low matter density, it is a smooth crossover, as predicted by lattice QCD [1]. It has been conjectured that a critical point (CP) exists in the nuclear matter phase diagram of temperature versus matter density between the first-order phase transition and smooth crossover [2–6]. The correlation length increases dramatically near the CP, causing large fluctuations in conserved quantities such as the net baryon number [7]. Searching for the CP is a subject of active research in heavy-ion collisions [8–17].

Light nuclei production is well-modeled by nucleon coalescence [18–25]. The coalescence model predicts that large baryon number fluctuations affect the production rate of light nuclei [26, 27]. For example, the production of tritons (t) is enhanced relative to that of deuterons (d) when there are extra fluctuations in the neutron density because a triton contains two neutrons (n), whereas a deuteron contains only one. As a result, the compound ratio $N_t N_p/N_d^2$ involving the multiplicities of protons (N_p), deuterons (N_d), and tritons (N_t) was enhanced. Similarly, the production of helium-3 (*he*) and the ratio of $N_{he} N_n/N_d^2$ increased with respect to extra fluctuations in the proton density.

Following Ref. [26–28], the average deuteron multiplicity density in the coalescence model is given by

This work was supported in part by the U.S. Department of Energy (No. DE-SC0012910), National Nature Science Foundation of China (Nos. 12035006 and 12075085), and the Ministry of Science and Technology of China (No. 2020YFE020200).

✉ An Gu
03302@zjhu.edu.cn

1 Huzhou University, Huzhou 313000, China

2 Purdue University, West Lafayette, IN 47907, USA

3 Livermore High School, Livermore, CA 94550, USA

$$\bar{n}_{\rm d}\Big/\left(\frac{3}{\sqrt{2}}A\right) = \langle(\bar{n}_{\rm p}+\delta n_{\rm p})(\bar{n}_{\rm n}+\delta n_{\rm n})\rangle = \bar{n}_{\rm p}\bar{n}_{\rm n} + \langle\delta n_{\rm p}\delta n_{\rm n}\rangle = \bar{n}_{\rm p}\bar{n}_{\rm n}(1+(\alpha\Delta n_{\rm n})_{\rm d}), \tag{1}$$

where the protons and neutrons are assumed to be in thermal equilibrium with an effective temperature $T_{\rm eff}$, and $A=\left(\frac{2\pi}{m_N T_{\rm eff}}\right)^{3/2}$ is the shorthand notation (m_N is the nucleon mass). Here $\bar{n}$ denotes the average density. The neutron density fluctuations are denoted as

$$\Delta n_{\rm n} = \langle(\delta n_{\rm n})^2\rangle/\bar{n}_{\rm n}^2, \tag{2}$$

and $\alpha = \frac{\langle\delta n_{\rm p}\delta n_{\rm n}\rangle}{\bar{n}_{\rm p}\bar{n}_{\rm n}}/\Delta n_{\rm n} = \frac{\bar{n}_{\rm n}}{\bar{n}_{\rm p}}\frac{\langle\delta n_{\rm p}\delta n_{\rm n}\rangle}{\langle(\delta n_{\rm n})^2\rangle}$ denotes the correlations between proton and neutron number fluctuations. If the proton and neutron numbers fluctuate independently, $\alpha=0$; if they fluctuate simultaneously, $\alpha=1$. It is noteworthy that we have thus far neglected the details of deuteron formation, which is determined by the deuteron wavefunction and is often implemented by the Wigner function formalism (see below). The fluctuations affecting deuteron formation are those within the typical volumes of deuterons. We note this in Eq. (1) by the subscript 'd' in $(\alpha\Delta n_{\rm n})_{\rm d}$ to indicate that it is the average $\alpha\Delta n_{\rm n}$ within the typical deuteron size that is relevant.

Similarly, the triton average multiplicity density is given by

$$\bar{n}_{\rm t}/\left(\frac{3\sqrt{3}}{4}A^2\right) = \langle(\bar{n}_{\rm p}+\delta n_{\rm p})(\bar{n}_{\rm n}+\delta n_{\rm n})^2\rangle = \bar{n}_{\rm p}\bar{n}_{\rm n}^2(1+(\Delta n_{\rm n})_{\rm t}+2(\alpha\Delta n_{\rm n})_{\rm t}+(\beta\Delta n'_{\rm n})_{\rm t}), \tag{3}$$

where $\Delta n'_{\rm n} = \langle(\delta n_{\rm n})^3\rangle/\bar{n}_{\rm n}^3$ and $\beta = \frac{\langle\delta n_{\rm p}(\delta n_{\rm n})^2\rangle}{\bar{n}_{\rm p}\bar{n}_{\rm n}^2}/\Delta n'_{\rm n} = \frac{\bar{n}_{\rm n}}{\bar{n}_{\rm p}}\frac{\langle\delta n_{\rm p}(\delta n_{\rm n})^2\rangle}{\langle(\delta n_{\rm n})^3\rangle}$. Similar to α in Eq. (1), the β parameters denote the three-body correlations. When the proton and neutron numbers fluctuate independently, $\beta=0$, and when they fluctuate together, $\beta=1$. The subscript 't' in Eq. (3) indicates that only fluctuations averaged within the typical volume of the triton size matter. Note that in Eq. (3), we simply write $n_{\rm n}^2$ for the neutron pair density; however, for an identical particle pair, the multiplicity is $N(N-1)$, so the pair fluctuations of Eq. (2) should be understood as those beyond Poisson fluctuations.

Thus, the compound ratio is given by

$$\frac{N_{\rm p}N_{\rm t}}{N_{\rm d}^2} = \frac{\bar{n}_{\rm p}\bar{n}_{\rm t}}{\bar{n}_{\rm d}^2} = \frac{1+(\Delta n_{\rm n})_{\rm t}+2(\alpha\Delta n_{\rm n})_{\rm t}+(\beta\Delta n'_{\rm n})_{\rm t}}{2\sqrt{3}(1+(\alpha\Delta n_{\rm n})_{\rm d})^2}. \tag{4}$$

If one neglects α and β, then Eq. (4) is reduced to

$$\frac{N_{\rm p}N_{\rm t}}{N_{\rm d}^2} \approx \frac{1}{2\sqrt{3}}(1+(\Delta n_{\rm n})_{\rm t}), \tag{5}$$

as in Ref. [26, 27]. Note that the factor $1/2\sqrt{3}$ originates from the thermal equilibrium assumption of nucleon abundances. Therefore, the $N_{\rm t}N_{\rm p}/N_{\rm d}^2$ may be a good measure of neutron density fluctuations, a large value of which can signal the CP.

A unique signature of the CP is the nonmonotonic behavior of the ratio $N_{\rm t}N_{\rm p}/N_{\rm d}^2$ in the beam energy, where a peak of the ratio in a localized region of beam energy can signal large neutron fluctuations and the CP [26, 27]. The STAR experiment at RHIC recently observed nonmonotonic behavior of the $N_{\rm t}N_{\rm p}/N_{\rm d}^2$ ratio in the top 10% of central Au+Au collisions as a function of the nucleon–nucleon center-of-mass energy ($\sqrt{s_{\rm NN}}$) in the Beam Energy Scan (BES) data [29].

A nonmonotonic bump was observed in the ratio localized in the energy region $\sqrt{s_{\rm NN}} = 20-30$ GeV. It should be noted that the local bump is prominent in the $N_{\rm t}N_{\rm p}/N_{\rm d}^2$ ratio of the extrapolated yields to all transverse momenta ($p_{\rm T}$) but not as prominent in the measured fiducial range of $0.5 < p_{\rm T}/A < 1.0$ GeV/c and $0.4 < p_{\rm T}/A < 1.2$ GeV/c (where A is the mass number corresponding to each light nucleus in the ratio) [29].

This is illustrated in the left panels of Fig. 1 where the STAR-measured $N_{\rm t}N_{\rm p}/N_{\rm d}^2$ ratios from the total extrapolated yields and two measured $p_{\rm T}/A$ ranges are reproduced. The "extrapolation factor" (f), that is, the $N_{\rm t}N_{\rm p}/N_{\rm d}^2$ ratio of the total light nuclei yields extrapolated to the entire $p_{\rm T}/A$ range [0–∞) divided by the ratio of those measured within a fiducial $p_{\rm T}/A$ range, is shown in the right panel of Fig. 1 for the two measured $p_{\rm T}/A$ ranges. It should be noted that the integrated yields of protons, deuterons, and tritons over the full momentum space in the STAR experiment were extrapolated from slightly different ranges of the scaled transverse momentum $p_{\rm T}/A$. The aforementioned ratio for the measured fiducial range was obtained using particle yields within the same $p_{\rm T}/A$ range as in the STAR experiment. The statistical uncertainties between the fiducial yield of a given $p_{\rm T}$ spectrum and the extrapolated total yield are correlated, as are the systematic uncertainties. Thus, the statistical and systematic uncertainties are considered to be the quadratic *difference* of the corresponding uncertainties in the $N_{\rm t}N_{\rm p}/N_{\rm d}^2$ between the fiducial $p_{\rm T}/A$ and total ranges. As expected from the STAR results [29], the f values peaked in the $\sqrt{s_{\rm NN}}$ = 20–30 GeV range and were nonmonotonic; the nonmonotonic effect was of the order of 10%.

In this study, we use a toy model to generate nucleons and form d, t, and ^{3}He by using a coalescence model. We study the ratios of the light nuclei yields as functions of the magnitude of neutron multiplicity fluctuations and examine

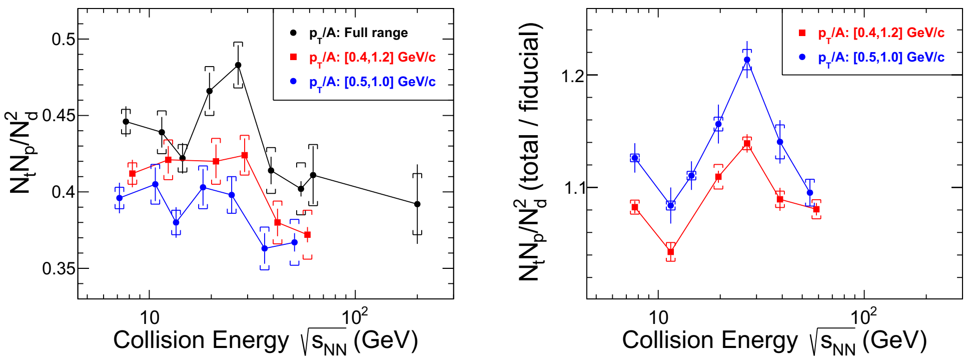

Fig. 1 (Color online) (Left) The N_tN_p/N_d^2 ratio in 0–10% central Au+Au collisions as functions of beam energy $\sqrt{s_{NN}}$ measured by STAR [29]. The ratio of the extrapolated total yields and those from two measured p_T/A ranges are shown. The ratios from the measured p_T/A ranges are shifted in the horizontal axis for clarity. (Right) The extrapolation factor f, i.e., the N_tN_p/N_d^2 ratio from the extrapolated total yields divided by that from the fiducial yields in a given measured p_T/A range, is shown for the two measured p_T/A ranges as functions of $\sqrt{s_{NN}}$. The statistical and systematic uncertainties on f are the quadratic *difference* of the corresponding uncertainties of the N_tN_p/N_d^2 ratio between the given measured p_T/A range and the total range. The rightmost square is shifted in the horizontal axis for clarity

the role of p_T acceptance in these ratios. First, we confined ourselves to a simple toy model to gain insight. We then attempted to conduct more realistic simulations mimicking STAR BES data to examine what STAR measurements may entail.

2 Coalescence model

The probability of forming a composite particle from particle 1 at position $\vec{r}_1$ with momentum $\vec{p}_1$ and particle 2 at position $\vec{r}_2$ with momentum $\vec{p}_2$ is estimated using the Wigner function:

$$W(\vec{r}_1,\vec{p}_1,\vec{r}_2,\vec{p}_2) = g \cdot 8\exp\left(-\frac{r_{12}^2}{\sigma_r^2} - \frac{p_{12}^2}{\sigma_p^2}\right), \qquad (6)$$

where

$$r_{12} = |\vec{r}_1 - \vec{r}_2|,$$
$$p_{12} = \mu\left|\frac{\vec{p}_1}{m_1} - \frac{\vec{p}_2}{m_2}\right|,$$

and $\mu = \frac{m_1 m_2}{m_1+m_2}$ denote the reduced mass of a two-body system. The parameter σ_r is the characteristic coalescence size in the configuration space and $\sigma_p = 1/\sigma_r$ (where $\hbar = c = 1$) is that in the momentum space.

Based on the Wigner function expressed in Eq. (6), the root-mean-square (RMS) radius of the coalesced composite particle is calculated as $R = \frac{\sqrt{3m_1m_2/2}}{m_1+m_2}\sigma_r$. Therefore, the coalescence parameter σ_r can be determined from the particle size as follows:

$$\sigma_r = \frac{m_1+m_2}{\sqrt{3m_1m_2/2}}R\,. \qquad (7)$$

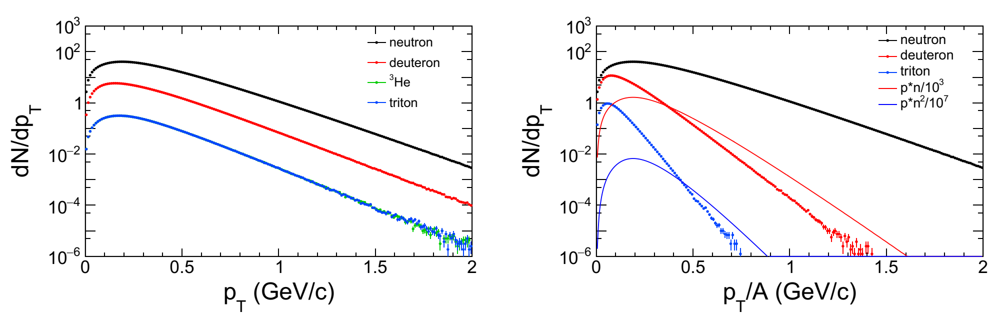

Fig. 2 (Color online) (Left) Transverse momentum p_T spectra of deuteron, ^{3}He and triton calculated by the coalescence model from a system of average $\bar{N}_p = 20$ protons and $\bar{N}_n = 20$ neutrons at "temperature" $T = 150$ MeV (Eq. (9)) randomly distributed within a cylinder of 10 fm radius and 10 fm length. No extra fluctuations are included beyond Poisson, i.e., $\theta = 1$. (Right) The same spectra plotted as functions of p_T/A (A is the corresponding mass number). Superimposed in curves are the products of $(dN_p/dp_T) \times (dN_n/dp_T)$ and $(dN_p/dp_T) \times (dN_n/dp_T)^2$ at the same p_T/A value, arbitrarily scaled to compare to the shapes of the deuteron and triton spectra, respectively

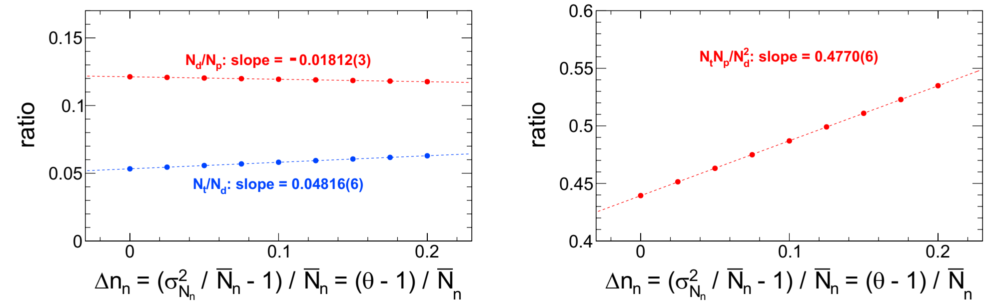

Fig. 3 (Color online) Yield ratios of $N_\mathrm{d}/N_\mathrm{p}$ and $N_\mathrm{t}/N_\mathrm{d}$ (left) and $N_\mathrm{t}N_\mathrm{p}/N_\mathrm{d}^2$ (right) as functions of Δn_n of Eq. (10), the magnitude of neutron multiplicity fluctuations beyond Poisson. Numbers inside the parentheses indicate the uncertainty to the corresponding last digit. The light nuclei are formed by coalescence from a system of average $\bar{N}_\mathrm{p} = 20$ protons and $\bar{N}_\mathrm{n} = 20$ neutrons at $T = 150$ MeV (Eq. (9)) randomly distributed within a cylinder of 10 fm radius and 10 fm length

Deuterons coalesce with protons and neutrons. The RMS size of the deuteron is $R_\mathrm{d} = 1.96$ fm [30], so for deuteron $\sigma_\mathrm{r} = \sqrt{\frac{8}{3}}R_\mathrm{d} = 3.20$ fm. The triton (helium-3) is formed by the coalescence of a deuteron and neutron (proton), following the same prescription as Eq. (6). The triton RMS size is $R_\mathrm{t} = 1.59$ fm [30]. Therefore, for triton, $\sigma_\mathrm{r} = \sqrt{3}R_\mathrm{t} = 2.75$ fm. For ^{3}He, we also assume $\sigma_\mathrm{r} = 2.75$ fm to be symmetric.

The $g$factor represents the probability of the proper total spin of the composite particle.

$$g = (2S+1)/\Pi_{i=1}^{2}\left(2s_i+1\right), \tag{8}$$

where S is the spin of the composite particle (1 for d, 1/2 for both t and ^{3}He), and s_i is the spin of each coalescing particle. For the d formed from p and n, the g-factor was 3/4. For t (^{3}He), formed from d and n (p), it is 1/3.

3 Toy-model simulation details

A system of nucleons was generated using a toy model. The nucleons were assumed to be uniformly distributed in a cylinder of 10 fm length and 10 fm radius. The transverse momentum spectra of the nucleons were assumed to be

$$\mathrm{d}N/\mathrm{d}p_\mathrm{T} \propto p_\mathrm{T}\exp(-p_\mathrm{T}/T), \tag{9}$$

where the "temperature" parameter is set to $T = 150$ MeV. Note that Eq. (9) is not a thermal distribution for massive particles; we use the term "temperature" for convenience. The azimuthal angle of the momentum vector was uniformly distributed between 0 and 2π. The pseudorapidity η was assumed to be uniform between -1 and 1. The use of rapidity or pseudorapidity was insignificant.

In this study, we did not use a thermal model to predict the average multiplicity; rather, we set the average multiplicities of protons and neutrons to $\bar{N}_\mathrm{p} = \bar{N}_\mathrm{n} = 20$. This is simple, because our goal was to study only the effects of neutron multiplicity fluctuations. Therefore, the baseline of the $N_\mathrm{t}N_\mathrm{p}/N_\mathrm{d}^2$ ratio is not $1/2\sqrt{3}$ but is rather determined by the ratio of the degeneracy g factors as $\frac{1}{3}\cdot\frac{3}{4}/\left(\frac{3}{4}\right)^2 = \frac{4}{9}$ [31].

We assigned Poisson fluctuations to the number of protons and only varied the fluctuation magnitude for the number of neutrons (we focused on the compound ratio $N_\mathrm{t}N_\mathrm{p}/N_\mathrm{d}^2$). The latter is achieved by using negative binomial distributions $P(N_\mathrm{n} = k) = C_k^{k+r-1}(1-p)^k p^r$, where r and p are free parameters.

The mean and variance are $\bar{N}_\mathrm{n} = \frac{r(1-p)}{p}$ and $\sigma^2_{N_\mathrm{n}} = \frac{r(1-p)}{p^2}$, respectively. The fluctuation magnitude is given by $\sigma^2_{N_\mathrm{n}} = \bar{N}_\mathrm{n}/p \equiv \theta\bar{N}_\mathrm{n}$ (where $\theta \equiv 1/p \geq 1$), which is always larger than Poisson fluctuations unless the probability $p = 1$ when the negative binomial distribution is reduced to Poisson. We used p to control the magnitude of the fluctuations in N_n and selected the proper r value to obtain the desired average neutron multiplicity, $\bar{N}_\mathrm{n}$.

It is worth noting that we utilized fluctuations in the total number of neutrons N_n event-by-event to mimic fluctuations in the local neutron number density. The purpose of our study is to investigate the behavior of $N_\mathrm{t}N_\mathrm{p}/N_\mathrm{d}^2$ as a function of the neutron density fluctuation magnitude but not to suggest that density fluctuations are caused by fluctuations in the total multiplicity. In our simulation, given a total N_n in an event, the neutrons were randomly distributed in the cylinder volume. The fluctuations in N_n determine the magnitude of the neutron density fluctuations, which is averaged over the entire volume. In other words, Δn_n in Eq. (2) can be quantified by fluctuations in N_n beyond Poisson,

$$\Delta n_\mathrm{n} = (\sigma^2_{N_\mathrm{n}}/\bar{N}_\mathrm{n} - 1)/\bar{N}_\mathrm{n} \equiv (\theta - 1)/\bar{N}_\mathrm{n}\,. \tag{10}$$

Note that θ quantifies the fluctuations in N_n in the unit of Poisson fluctuations, and $\theta - 1$ quantifies those beyond Poisson fluctuations.

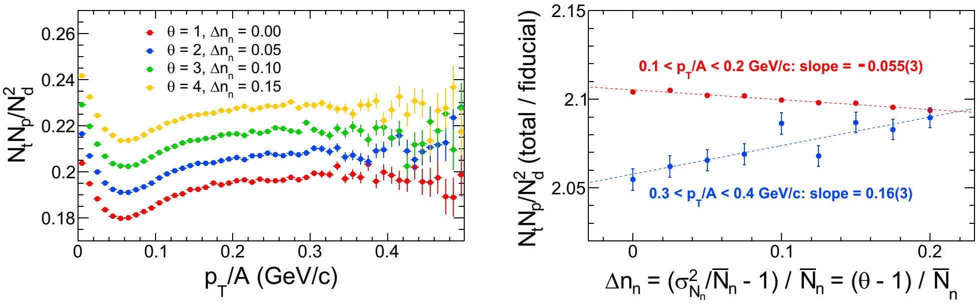

Fig. 4 (Color online) (Left) The N_tN_p/N_d^2 ratio as functions of p_T/A. (Right) The N_tN_p/N_d^2 extrapolation factor f from $p_T/A = 0.1-0.2$ GeV/c and 0.3–0.4 GeV/c as a function of Δn_n. The light nuclei are formed by coalescence from a system of average $\bar{N}_p = 20$ protons and $\bar{N}_n = 20$ neutrons at $T = 150$ MeV (Eq. (9)) randomly distributed within a cylinder of 10 fm radius and 10 fm length

In total, 1.6×10^8 events were simulated. Deuterons, tritons, and helium-3 were formed by coalescence. For each event, the deuteron formation via double loops over protons and neutrons was considered. For each deuteron, the formation of t and ^{3}He was implemented by looping over the remaining nucleons. The nucleons were randomly reordered such that the probabilities of forming t and ^{3}He were unbiased. A random number uniformly distributed between 0 and 1 was used to determine whether the two particles coalesced into a light nucleus. If the random number is smaller than the Wigner function value in consideration, the corresponding light nucleus is formed. Once a light nucleus formed, the coalescing particles were removed from further consideration.

4 Toy-model simulation results and discussions

Figure 2 shows the p_T spectra of the generated neutrons and the coalesced d, t, and ^{3}He in the left panel, and the right panel those spectra in the scaled p_T/A. No extra fluctuations are included beyond Poisson in this figure (i.e., $\theta = 1$); therefore, the proton spectrum is identical to that of neutrons. In the right panel, the product of the proton and neutron spectra and the product of the proton and squared neutron spectra are shown as smooth histograms. These products are the corresponding d and t spectra if the coalescence parameters $\sigma_p = 0$ and $\sigma_r = \infty$ in Eq. (6). The coalesced d and t spectra are steeper than those of the products because of the finite σ_p and σ_r implemented in our coalescence model.

Figure 3 shows in the left panel the yield ratios of N_d/N_p and N_t/N_d as functions of the neutron fluctuation magnitude Δn_n in Eq. (10). The N_t/N_d ratio increases with Δn_n, which is consistent with the expected stronger effect of the neutron density fluctuations on t than on d production. The N_d/N_p ratio decreases slightly, but is statistically significant. This is counterintuitive, as one would expect no dependence because $\bar{N}_n$ is the same for all values of Δn_n; events with more neutrons would be balanced out by those with fewer neutrons in terms of deuteron production. However, $\bar{N}_p = 20$ is fixed, and the fluctuations in N_p are treated as uncorrelated with those in N_n in our study. The production of deuterons will be "saturated" in events with large N_n—those neutrons would not get "equal" share of protons to form deuterons. Consequently, N_d/N_p is smaller for a larger Δn_n.

The right panel of Fig. 3 shows the N_tN_p/N_d^2 ratio as a function of Δn_n. The N_tN_p/N_d^2 clearly increases with Δn_n. The slope was approximately 0.477, significantly nonzero, and the intercept was approximately 0.439. These values are approximately equal to the expected degeneracy factor of 4/9. The slight deviations may be due to the different size parameters of the deuterons and triton as the Wigner function parameters differ.

As previously mentioned, the measured nonmonotonic feature of the N_tN_p/N_d^2 ratio as a function of the beam energy $\sqrt{s_{NN}}$ by STAR appears to depend on the considered p_T/A range [29], which is stronger for the extrapolated yield ratio than for those with limited p_T/A acceptance. Therefore, it is important to investigate whether a nonmonotonic extrapolation factor can result from trivial physics, such as nucleon spectral shape changes as a function of the beam energy. To this end, we first examined the N_tN_p/N_d^2 as a function of p_T/A in our toy-model simulation. This is shown in Fig. 4 left panel shows the various θ values. In the extreme case of coalescence with an identical momentum, the N_tN_p/N_d^2 was independent of p_T. The falling and rising characteristics of the shape are determined by the p_T-distribution in Eq. (9) and the coalescence parameters of the light nuclei. The shapes are similar for various fluctuation magnitudes, and the overall ratio increases with θ as expected. The right panel of Fig. 4 shows extrapolation factor f as a function of Δn_n. (Note that the total yields in simulation are known of course, not from extrapolation, but we keep use of the term "extrapolation factor.") Two fiducial ranges are depicted: $p_T/A = 0.1-0.2$ and 0.3–0.4 GeV/c. The extrapolation factor f varies with Δn_n; however, the variation is relatively small, less than 1% for the $p_T/A = 0.3$–0.4 GeV/c range for $\theta = 2$, which is the fluctuation magnitude of a factor of 2 of that of Poisson. This implies that even when there are enhanced fluctuations in a local region in the beam energy $\sqrt{s_{NN}}$, the extrapolation factor remains approximately the same and does not cause a change in the shape of the N_tN_p/N_d^2 ratio vs. $\sqrt{s_{NN}}$ from the limited p_T range to the extrapolated full p_T range. However, we examined only relatively narrow p_T/A ranges at small p_T/A values because of statistical considerations. The fiducial p_T/A ranges in the STAR analysis are relatively large and wide. Therefore, no direct comparisons can be made between our study and the STAR results thus far.

5 More realistic simulations

In heavy-ion collisions, p_T distributions can be significantly altered by the collective radial flow. The shape of the p_T distribution affects the N_tN_p/N_d^2 ratio as a function of p_T/A. To investigate the effect of the nucleon p_T spectral shape on the extrapolation factor of the N_tN_p/N_d^2 ratio, we first vary the temperature parameter T in Eq. (9). Figure 5 shows the T-dependence of the extrapolation factotr f for $p_T/A = 0.3$–0.4 GeV/c, with a given neutron fluctuation of $\Delta n_n = 0.1$ (i.e., $\theta = 3$). As expected, the f value varies with T as expected, and the variation is monotonic. Thus, the T-dependent p_T spectral shape does not cause an artificial nonmonotonic N_tN_p/N_d^2 enhancement from limited to full p_T acceptance in any given localized T range and, correspondingly, the beam energy range.

The collective radial flow in heavy-ion collisions creates a correlation between the momentum of a particle and its freeze-out radial position. This correlation is not present in the above simulations, but can be important for coalescence. To fully comprehend the implications of STAR data [29], we performed simulations using more realistic kinematic distributions. We obtained freeze-out information from the measured data [32, 33] as described below. The other simulation details are the same as those described in Sect. 3.

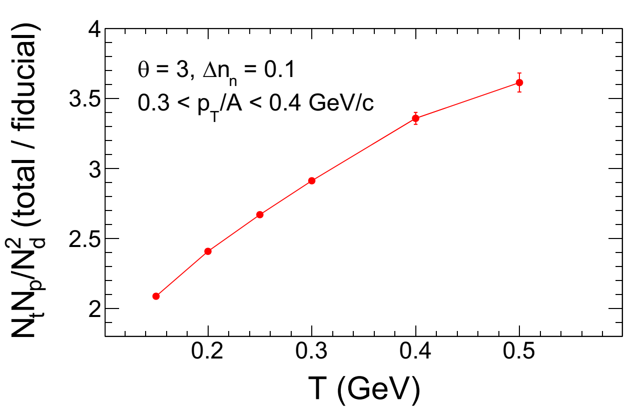

Fig. 5 (Color online) The N_tN_p/N_d^2 "extrapolation factor" for the $p_T/A = 0.3$–0.4 GeV/c acceptance as a function of T, with $\theta = 3$ or $\Delta n_n = 0.1$. The light nuclei are formed by coalescence from a system of average $\bar{N}_p = 20$ protons and $\bar{N}_n = 20$ neutrons randomly distributed within a cylinder of 10 fm radius and 10 fm length

The charged hadron mulitplicity N_{ch}, the inclusive proton multiplicity density dN_p/dy, the chemical freeze-out temperature T_{chem} and volume ($V_{chem} \equiv \frac{4\pi}{3}R^3_{sphere}$), the kinematic freeze-out temperature T_{kin}, and the average collective radial flow velocity $\langle\beta\rangle$ in the blast wave parameterization have been reported for the STAR experiment using various beam energies [32, 33]. We concentrate only on the central 0–5% collisions and parameterize the freeze-out quantities as functions of N_{ch}. The parameters have fit uncertainties; however, because we were only interested in the input values in our simulation to study light nuclei coalescence, we simply used the parameterized values.

- The measured dN_p/dy is shown in Fig. 6 (upper left) as a function of N_{ch}. The measured protons originate from two sources: transport protons whose abundance decreases with energy, and produced protons whose abundance increases with energy. We thus parameterize dN_p/dy by combination of two functions, one decreasing and the other increasing with N_{ch}. The parameterization is given by $dN_p/dy = 318e^{-N_{ch}/148} + 68N_{ch}^{1.4}$, as superimposed.
- The chemical freeze-out temperature T_{chem} is shown in Fig. 6 (upper right) as a function of N_{ch}. The T_{chem} increases with N_{ch} and then saturates, so we parameterize it by $T_{chem} = 167(1 - e^{-N_{ch}/144})$ MeV.
- The effective sphere radius for the chemical freeze-out volume appears linear in $N_{ch}^{1/3}$, so we parameterize it as $R_{sphere} = 3.1 + 0.42N_{ch}^{1/3}$. We allow the intercept to be a free parameter because the fit is otherwise not as good.
- The kinetic freeze-out temperature T_{kin} is shown in Fig. 6 (lower left) as a function of N_{ch}. It is found to decrease with N_{ch} and parameterized by $T_{kin} = 142e^{-N_{ch}/1827}$ MeV.
- The average radial flow velocity is shown in Fig. 6 (lower right) as a function of N_{ch}. It increases with N_{ch} and appears to saturate at large N_{ch}, so we parameterize it as $\langle\beta\rangle = 0.6(1 - e^{-N_{ch}/241})$.

The information on the nucleons to be input into the coalescence model is that of kinetic freeze-out. The kinetic freeze-out volume V_{kin} is obtained by assuming the system expands adiabatically, so $V_{kin}/V_{chem} = (T_{chem}/T_{kin})^{3/2}$. In our simulation, we assumed that the collision zone was a cylinder with a radius $R = 7$ fm, and the length of the cylinder was determined by $V_{kin}/(\pi R^2)$. Protons and neutrons were

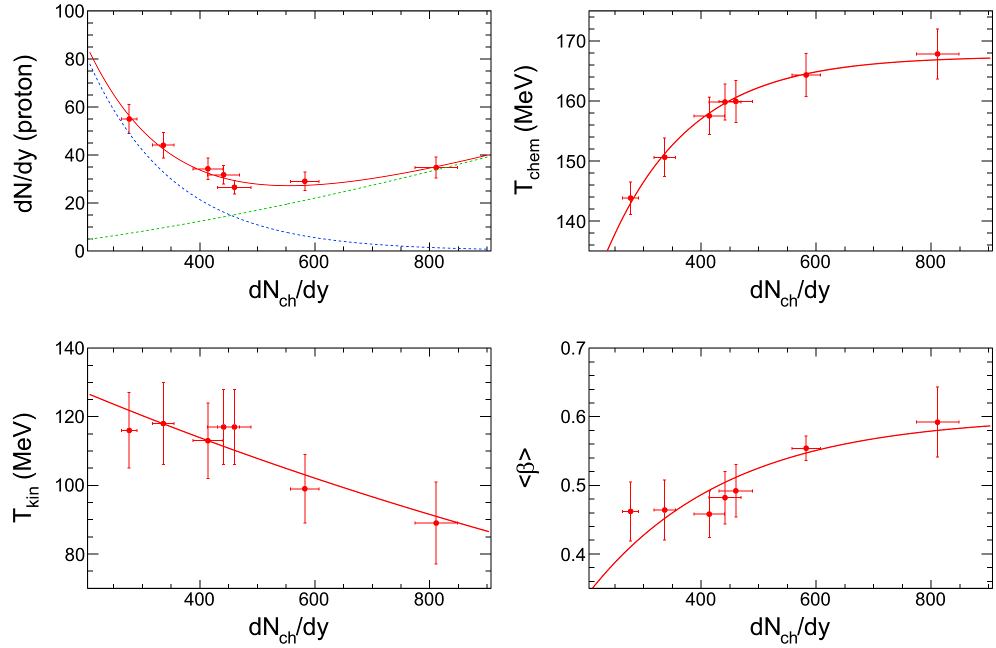

Fig. 6 (Color online) The measured proton multiplicity density $\mathrm{d}N_{\mathrm{p}}/\mathrm{d}y$ (upper left), the chemical freeze-out temperature T_{chem} (upper right), the kinetic freeze-out temperature T_{kin} (lower left), and the average radial velocity $\langle\beta\rangle$ (lower right) as functions of the charged hadron multiplicity density $\mathrm{d}N_{\mathrm{ch}}/\mathrm{d}y$ [32, 33]. The parameterizations to the data are superimposed and used as inputs to our simulations

positioned uniformly and randomly inside the cylinder. The mean numbers of protons and neutrons were assumed to be $\bar{N}_{\mathrm{p}} = \bar{N}_{\mathrm{n}} = 2 \times \mathrm{d}N_{\mathrm{p}}/\mathrm{d}y$ over two units of speed. Protons and neutrons were first generated according to the thermal distribution at T_{kin}.

$$\mathrm{d}N/\mathrm{d}p_{\mathrm{T}} \propto p_{\mathrm{T}} m_{\mathrm{T}} e^{-m_{\mathrm{T}}/T}\,. \tag{11}$$

The generated protons and neutrons are boosted radially with a boost velocity dependent on the radial position of the nucleon (r) within the cylinder:

$$\beta = \beta_{\mathrm{s}}(r/R)^n\,, \tag{12}$$

where the surface velocity is $\beta_{\mathrm{s}} = (1 + n/2)\langle\beta\rangle$. In this study, the parameter n for all the collision energies was set to 1.

Figure 7 shows the calculated p_{T}/A spectra of triton as an example for selected beam energies for $\theta = 1$ and $\theta = 10$. The p_{T}/A spectra had the same shape for $\theta = 1$ and $\theta = 10$ for a given beam energy. The right panel shows the yield fractions of the protons (red), deuterons (blue), and triton (green) in the limited p_{T} range of $0.5 < p_{\mathrm{T}}/A < 1.0\,\mathrm{GeV}/c$. It is interesting to note that while the proton fiducial yield fraction steadily decreases with the beam energy, as expected

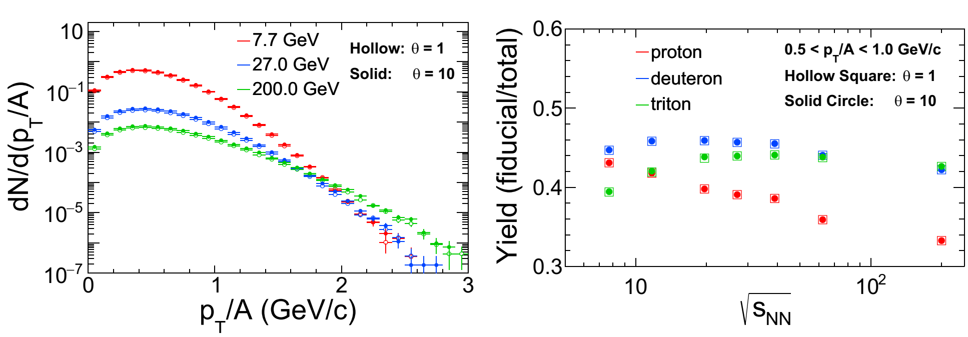

Fig. 7 (Color online) (Left panel) The p_{T}/A spectra of triton for different beam energies. Two values of θ are shown: $\theta = 1$ for Poisson (hollow markers) and $\theta = 10$ for enhanced neutron fluctuations (filled markers). (Right panel) The yield fractions of proton (red), deuteron (blue), and triton (green) within $0.5 < p_{\mathrm{T}}/A < 1.0$ GeV/c as functions of $\sqrt{s_{\mathrm{NN}}}$ with $\theta = 1$ (open marker) and $\theta = 10$ (filled marker)

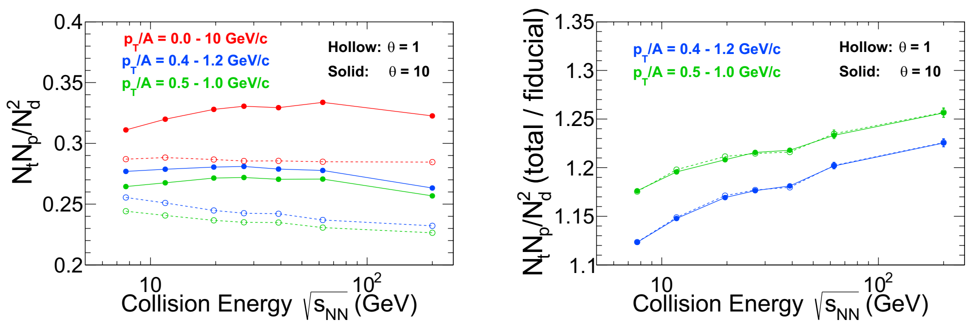

Fig. 8 (Color online) (Left panel) The N_tN_p/N_d^2 ratio as functions of $\sqrt{s_{NN}}$ for the entire p_T range (red) and for two limited p_T/A ranges (blue and green). Two values of θ are shown: $\theta = 1$ for Poisson (hollow markers) and $\theta = 10$ for enhanced neutron fluctuations (filled markers). (Right panel) The N_tN_p/N_d^2 extrapolation factor for the $p_T/A = 0.4 - 1.2$ GeV/c (blue) and 0.5−1.0 GeV/c (green) acceptance as functions of $\sqrt{s_{NN}}$, with $\theta = 1$ (hollow markers) and 10 (solid markers)

from the flattening of the proton p_T spectra, the deuteron and triton fiducial yield fractions first increase with the energy and then decrease. This is because the yields in the low $p_T/A < 0.5\,\mathrm{GeV}/c$ region are disproportionately more dominant at lower energies for the coalesced light nuclei, and more so for triton. However, no differences were observed in the yield fractions for $\theta = 1$ and $\theta = 10$. This implies that the yield extrapolations are the same for different fluctuation magnitudes. This, in turn, suggests that the effect of extrapolation on the N_tN_p/N_d^2 ratio is the same, independent of the fluctuation magnitude, as illustrated below.

Figure 8 left panel shows the N_tN_p/N_d^2 calculated using our coalescence model as a function of $\sqrt{s_{NN}}$. The ratios are shown for the entire p_T range and for the two limited p_T/A ranges measured by STAR: $0.4 < p_T/A < 1.2\,\mathrm{GeV}/c$ and $0.5 < p_T/A < 1.0\,\mathrm{GeV}/c$. The results for two values of θ are depicted: $\theta = 1$ corresponds to Poisson fluctuations in the neutron multiplicity, and $\theta = 10$ corresponds to enhanced fluctuations with a magnitude corresponding to ~ 10% increase in the measured N_tN_p/N_d^2 ratio by STAR (cf Eq. (10), where a typical $\bar{N}_n \sim 60$–100, as shown in Fig. 6). Similar to the STAR measurements [29], the calculated N_tN_p/N_d^2 ratios show weak energy dependence. The calculated N_tN_p/N_d^2 values were lower than the measured values.

The right panel of Fig. 8 shows the extrapolation factors f of the N_tN_p/N_d^2 from $p_T/A = 0.4 - 1.2\,\mathrm{GeV}/c$ and 0.5–1.0 GeV/c, respectively. The extrapolation increases monotonically with an increase $\sqrt{s_{NN}}$ and is smooth. For a given p_T/A range, the f values were almost identical for the two θ values; thus, we is so for all θ values we have simulated. The chosen $\theta = 10$ corresponds to $\Delta n_n = 0.1$ for $\bar{N}_n = 90$ only, which corresponds to different values of Δn_n at various beam energies. We checked our results for f using a fixed $\Delta n_n = 0.1$ value at all beam energies studied. No qualitative differences were observed between groups. Our results suggest that p_T-extrapolation alone does not create, enhance, or reduce a local peak in the N_tN_p/N_d^2 ratio as a function of $\sqrt{s_{NN}}$. In other words, the fluctuation increase in the $\sqrt{s_{NN}} \sim 20$–30 GeV region implied by the STAR-extrapolated N_tN_p/N_d^2 ratio [29] (such as a jump from the hollow red points to the solid red points at $\sqrt{s_{NN}} = 20$ –30 GeV in our simulation) should also be present in the ratios in the limited fiducial p_T/A regions (a jump from the hollow blue/green points to the solid blue/green points). Therefore, we postulate that the local peak in the extrapolated N_tN_p/N_d^2 in the STAR measurements [29] is unlikely to be caused by the physics of coalescence.

6 Summary

We simulated light nuclei production from a system of nucleons with varying magnitudes of neutron multiplicity fluctuations, Δn_n. It was found that the light nuclei yield ratio N_tN_p/N_d^2 increased linearly with Δn_n, confirming the findings of Ref. [26, 27]. We have further investigated the effect of finite acceptance by studying the "extrapolation factor" f for the N_tN_p/N_d^2 ratio as a function of Δn_n and the p_T spectra parameter T. The f value is found to be monotonic as a function of T and Δn_n; the variations in the latter were relatively small.

We also conducted a coalescence model study with realistic kinematic distributions of nucleons using measured freeze-out parameters, kinetic freeze-out temperature, and collective radial flow velocity. The N_tN_p/N_d^2 ratio was calculated using the coalescence model as a function of beam energy, and a weak beam energy dependence was found, similar to the experimental data. The extrapolation factor f was found to be smooth and monotonic in beam energy and independent of the magnitude of the neutron density fluctuations. We conclude that the extrapolation of the N_tN_p/N_d^2 ratio in p_T does not create, enhance, or reduce a local peak in the ratio of the beam energy. Therefore, our study suggests that the measured enhancement of the p_T-extrapolated N_tN_p/N_d^2 [29] is unlikely to be caused by coalescence.

Our study provides a necessary benchmark for light nuclei ratios as a probe for nucleon fluctuations, an important observation in the search for the critical point of nuclear matter. In the present study, we assumed that the fluctuations in the number of protons and neutrons were independent. One may implement varying degrees of correlation between these fluctuations and study their effects on N_tN_p/N_d^2. In addition, the effects of clustering or clumping [34–36], out-of-equilibrium effects [34], and feedback from excited states [37, 38] have not been considered. We leave these studies for future work.

Acknowledgements We thank Dr. Fuqiang Wang for suggesting the project and for the many fruitful discussions.

Author contributions All authors contributed to the study conception and design. Material preparation, data collection, and analysis were performed by An Gu and Michael X. Zhang. The first draft of the manuscript was written by An Gu, and all authors commented on the previous versions of the manuscript. All authors read and approved the final manuscript.

Data availability The data that support the findings of this study are openly available in Science Data Bank at https://cstr.cn/31253.11.sciencedb.15790 and https://www.doi.org/10.57760/sciencedb.15790.

Declarations

Conflict of interest The authors declare that they have no conflict of interest.

References

1. Y. Aoki, G. Endrodi, Z. Fodor et al., The Order of the quantum chromodynamics transition predicted by the standard model of particle physics. Nature **443**, 675–678 (2006). https://doi.org/10.1038/nature05120
2. A.M. Halasz, A.D. Jackson, R.E. Shrock et al., On the phase diagram of QCD. Phys. Rev. D **58**, 096007 (1998). https://doi.org/10.1103/PhysRevD.58.096007
3. M.A. Stephanov, K. Rajagopal, E.V. Shuryak, Signatures of the tricritical point in QCD. Phys. Rev. Lett. **81**, 4816–4819 (1998). https://doi.org/10.1103/PhysRevLett.81.4816
4. M.A. Stephanov, QCD phase diagram and the critical point. Prog. Theor. Phys. Suppl. **153**, 139–156 (2004). https://doi.org/10.1142/S0217751X05027965
5. K. Fukushima, T. Hatsuda, The phase diagram of dense QCD. Rept. Prog. Phys. **74**, 014001 (2011). https://doi.org/10.1088/0034-4885/74/1/014001
6. Y. Wu, X. Li, L. Chen et al., Several problems in determining the QCD phase boundary by relativistic heavy ion collisions. Nucl. Tech. (in Chinese) **46**, 040006 (2023). https://doi.org/10.11889/j.0253-3219.2023.hjs.46.040006
7. M.A. Stephanov, On the sign of kurtosis near the QCD critical point. Phys. Rev. Lett. **107**, 052301 (2011). https://doi.org/10.1103/PhysRevLett.107.052301
8. M.M. Aggarwal, Z. Ahammed, A.V. Alakhverdyants et al., An experimental exploration of the QCD phase diagram: the search for the critical point and the onset of de-confinement. https://doi.org/10.48550/arXiv.1007.2613
9. L. Adamczyk, J.K. Adkins, G. Agakishiev et al., Energy dependence of moments of net-proton multiplicity distributions at RHIC. Phys. Rev. Lett. **112**, 032302 (2014). https://doi.org/10.1103/PhysRevLett.112.032302
10. X. Luo, Exploring the QCD phase structure with beam energy scan in heavy-ion collisions. Nucl. Phys. A **956**, 75–82 (2016). https://doi.org/10.1016/j.nuclphysa.2016.03.025
11. A. Bzdak, S. Esumi, V. Koch et al., Mapping the phases of quantum chromodynamics with beam energy scan. Phys. Rept. **853**, 1–87 (2020). https://doi.org/10.1016/j.physrep.2020.01.005
12. S. Acharya, ALICE Collaboration et al., Global baryon number conservation encoded in net-proton fluctuations measured in Pb-Pb collisions at $\sqrt{s_{NN}}$ = 2.76 TeV. Phys. Lett. B **807**, 135564 (2020). https://doi.org/10.1016/j.physletb.2020.135564
13. J. Adamczewski-Musch, O. Arnold, C. Behnke et al., Proton-number fluctuations in $\sqrt{s_{NN}}$ =2.4 GeV Au + Au collisions studied with the High-Acceptance DiElectron Spectrometer (HADES). Phys. Rev. C **102**, 024914 (2020). https://doi.org/10.1103/PhysRevC.102.024914
14. J. Adam, L. Adamczyk, J.R. Adams et al., Nonmonotonic energy dependence of net-proton number fluctuations. Phys. Rev. Lett. **126**, 092301 (2021). https://doi.org/10.1103/PhysRevLett.126.092301
15. M. Abdallah, J. Adam, L. Adamczyk et al., Cumulants and correlation functions of net-proton, proton, and antiproton multiplicity distributions in Au+Au collisions at energies available at the BNL Relativistic Heavy Ion Collider. Phys. Rev. C **104**, 024902 (2021). https://doi.org/10.1103/PhysRevC.104.024902
16. M.S. Abdallah, B.E. Aboona, J. Adam et al., Measurements of proton high order cumulants in $\sqrt{s_{NN}}$ = 3 GeV Au+Au collisions and implications for the QCD critical point. Phys. Rev. Lett. **128**, 202303 (2022). https://doi.org/10.1103/PhysRevLett.128.202303
17. Y. Zhang, D. Zhang, X. Luo, Experimental study of the QCD phase diagram in relativistic heavy-ion collisions. Nucl. Tech. (in Chinese) **46**, 040001 (2023). https://doi.org/10.11889/j.0253-3219.2023.hjs.46.040001
18. S.T. Butler, C.A. Pearson, Deuterons from high-energy proton bombardment of matter. Phys. Rev. **129**, 836 (1963). https://doi.org/10.1103/PhysRev.129.836
19. H. Sato, K. Yazaki, On the coalescence model for high-energy nuclear reactions. Phys. Lett. B **98**, 153–157 (1981). https://doi.org/10.1016/0370-2693(81)90976-X
20. L.P. Csernai, J.I. Kapusta, Entropy and cluster production in nuclear collisions. Phys. Rept. **131**, 223–318 (1986). https://doi.org/10.1016/0370-1573(86)90031-1
21. C.B. Dover, U.W. Heinz, E. Schnedermann et al., Relativistic coalescence model for high-energy nuclear collisions. Phys. Rev. C **44**, 1636 (1991). https://doi.org/10.1103/PhysRevC.44.1636
22. R. Scheibl, U.W. Heinz, Coalescence and flow in ultrarelativistic heavy ion collisions. Phys. Rev. C **59**, 1585–1602 (1999). https://doi.org/10.1103/PhysRevC.59.1585
23. L.W. Chen, C.M. Ko, B.A. Li, Light clusters production as a probe to the nuclear symmetry energy. Phys. Rev. C **68**, 017601 (2003). https://doi.org/10.1103/PhysRevC.68.017601
24. Y. Oh, Z.W. Lin, C.M. Ko, Deuteron production and elliptic flow in relativistic heavy ion collisions. Phys. Rev. C **80**, 064902 (2009). https://doi.org/10.1103/PhysRevC.80.064902
25. K. Sun, L. Chen, K.C. Ming et al., Light nuclei production and QCD phase transition in heavy-ion collisions. Nucl. Tech. (in Chinese) **46**, 040012 (2023). https://doi.org/10.11889/j.0253-3219.2023.hjs.46.040012

26. K.J. Sun, L.W. Chen, C.M. Ko et al., Probing QCD critical fluctuations from light nuclei production in relativistic heavy-ion collisions. Phys. Lett. B **774**, 103–107 (2017). https://doi.org/10.1016/j.physletb.2017.09.056
27. K.J. Sun, L.W. Chen, C.M. Ko et al., Light nuclei production as a probe of the QCD phase diagram. Phys. Lett. B **781**, 499–504 (2018). https://doi.org/10.1016/j.physletb.2018.04.035
28. K.J. Sun, L.W. Chen, Analytical coalescence formula for particle production in relativistic heavy-ion collisions. Phys. Rev. C **95**, 044905 (2017). https://doi.org/10.1103/PhysRevC.95.044905
29. M. Abdulhamid et al., Beam energy dependence of triton production and yield ratio ($N_\mathrm{t} \times N_\mathrm{p}/N_\mathrm{d}^2$) in Au+Au collisions at RHIC. Phys. Rev. Lett. **130**, 202301 (2023). https://doi.org/10.1103/PhysRevLett.130.202301
30. G. Ropke, Light nuclei quasiparticle energy shift in hot and dense nuclear matter. Phys. Rev. C **79**, 014002 (2009). https://doi.org/10.1103/PhysRevC.79.014002
31. S. Wu, K. Murase, S. Tang et al., Examination of background effects on the light-nuclei yield ratio in relativistic heavy-ion collisions. Phys. Rev. C **106**, 034905 (2022). https://doi.org/10.1103/PhysRevC.106.034905
32. L. Adamczyk, J.K. Adkins, G. Agakishiev et al., Bulk properties of the medium produced in relativistic heavy-ion collisions from the beam energy scan program. Phys. Rev. C **96**, 044904 (2017). https://doi.org/10.1103/PhysRevC.96.044904
33. B.I. Abelev, M.M. Aggarwal, Z. Ahammed et al., Systematic measurements of identified particle spectra in pp, d^{+} Au and Au+Au collisions from STAR. Phys. Rev. C **79**, 034909 (2009). https://doi.org/10.1103/PhysRevC.79.034909
34. J. Steinheimer, J. Randrup, Spinodal amplification of density fluctuations in fluid-dynamical simulations of relativistic nuclear collisions. Phys. Rev. Lett. **109**, 212301 (2012). https://doi.org/10.1103/PhysRevLett.109.212301
35. E. Shuryak, J.M. Torres-Rincon, Baryon clustering at the critical line and near the hypothetical critical point in heavy-ion collisions. Phys. Rev. C **100**, 024903 (2019). https://doi.org/10.1103/PhysRevC.100.024903
36. K.J. Sun, W.H. Zhou, L.W. Chen, et al., Spinodal enhancement of light nuclei yield ratio in relativistic heavy ion collisions. https://doi.org/10.48550/arXiv.2205.11010
37. E. Shuryak, J.M. Torres-Rincon, Baryon preclustering at the freeze-out of heavy-ion collisions and light-nuclei production. Phys. Rev. C **101**, 034914 (2020). https://doi.org/10.1103/PhysRevC.101.034914
38. V. Vovchenko, B. Dönigus, B. Kardan et al., Feeddown contributions from unstable nuclei in relativistic heavy-ion collisions. Phys. Lett. B **809**, 135746 (2020). https://doi.org/10.1016/j.physletb.2020.135746